

Size Dependence of Melting Process of Armchair Hexagonal Boron Nitride Nanoribbon

Hang T. T. Nguyen^{1,2,†}, Tran Van Luong^{1,2} and Trinh T. Ngo³

¹Laboratory of Computational Physics, Faculty of Applied Science, Ho Chi Minh City University of Technology (HCMUT), Ho Chi Minh City, 268 Ly Thuong Kiet Street, District 10, Ho Chi Minh City, Vietnam

²Vietnam National University Ho Chi Minh City, Linh Trung Ward, Thu Duc District, Ho Chi Minh City, Vietnam

³Faculty of Education, An Giang University, 18 Ung Van Khiem Street, Dong Xuyen Ward, An Giang Province, Vietnam

E-mail: [†]hangbk@hcmut.edu.vn

Received 30 November 2023

Accepted for publication 18 April 2024

Published 6 June 2024

Abstract. *The dependence on the initial configuration size of armchair hexagonal boron nitride nanoribbon (h-BNNR) is investigated by molecular dynamics simulation. The initial configuration size of armchair h-BNNR containing 10000, 20000, and 30000 identical atoms of B and N is heated from 50 K to 6000 K via Tersoff potentials to study the dependence on the initial configuration size of the phase transition from crystal to liquid of armchair h-BNNR. Some results can be listed: the phase transition exhibits a first-order type; the phase transition from crystal to liquid states depends on the initial configuration size; the melting points of 10000, 20000, and 30000 atoms are 3640 K, 4000 K, and 4400 K, respectively; the dependence on the heating rate of the armchair h-BNNR is considered for the case of 20000 atoms; in this study range, the melting point decreases as the heating rate decreases; the atomic mechanism of the melting process is studied by analyzing the parameter and the appearance of the liquid-like atoms based on the critical value ; the critical value is used to classify solid-like and liquid-like atoms; the appearance of liquid-like atoms upon heating starts from the edges and grows inward; at the phase transition temperature, almost the entire crystal structure of the armchair h-BNNR configuration collapses.*

Keywords: melting of armchair hexagonal boron nitride nanoribbon; size dependence; heating rate dependence; formation of liquid-like atoms.

Classification numbers: 61.72.Cc; 64.70.dj.

1. Introduction

Boron nitride (BN) material has undergone extensive theoretical and experimental research due to its unique characteristics. These properties include a wide bandgap, exceptional strength, high thermal conductivity, high melting point, and applications as lubricants and adhesives, etc. [1]. As a result, BN finds applications in diverse fields, ranging from biomedicine [2] to electronic devices [3], including humidity sensing probes [4], DNA nucleotide detection [5], rapid analysis of Carbendazim in agriculture [6], cataluminescence gas sensors [7], photodetectors [8], field-effect transistors [9], and protective coatings [10]. BN can exist in different forms, such as amorphous, hexagonal, cubic, and wurtzite. One can see that hexagonal BN (h-BN) plays a particular role due to its unique properties, such as weak interactions between layers, chemical stability, and high polarization along the plane [1].

In contrast to graphene, h-BN is an insulator with a high bandgap, making it suitable for charge fluctuation platforms [11] and gate dielectrics [12]. It also serves as a natural hyperbolic and van der Waals material, allowing it to be combined with other materials to create hyperbolic infrared metasurface devices [13]. In addition, h-BN can form lateral graphene/h-BN heterostructures [14]. Furthermore, h-BN's mechanical properties remain nearly unchanged from monolayers to few-layer structures, making it an ideal candidate for mechanical reinforcements, in contrast to graphene, which experiences decreased mechanical properties with increasing layer thickness [15].

From the h-BN monolayer, various configurations can be tailored, such as nanoscrolls, nanotubes, nanoflakes, and nanoribbons. In particular, h-BN nanoribbon (h-BNNR) inherits properties from the h-BN monolayer while also being influenced by edge chirality (armchair and zigzag) [16]. Armchair h-BNNR exhibits remarkable thermoelectric properties, surpassing those of zigzag h-BNNRs. Additionally, the electrical and magnetic properties of h-BNNRs are sensitive to doping with organic molecules at the edges [17]. For instance, doping iron at the armchair edge alters electron transport parameters, while adsorbing nonmetallic atoms at the zigzag edge adjusts electrical and magnetic properties. Particularly for the h-BNNR zigzag, we have investigated in detail the atomic mechanism of the phase transition and determined the phase transition temperature to be about 4522 K [18].

In this study, the dependence of the thermal properties on the initial configuration size of armchair h-BNNR is studied using molecular dynamic simulation. Besides, the dependence on heating rate is also considered in this work to contribute to our understanding of the properties of BN materials. The phase transition from the crystal to a liquid state is observed. The atomic mechanism of the melting process is analyzed using various thermodynamic quantities related to the melting process. Details on the calculation scheme are shown in Sec. 2. Results and discussions related to the thermodynamics and atomic mechanism of melting armchair h-BNNR can be found in Sec. 3. Conclusions are given in the last section of the paper.

2. Calculation Details

As is well-known, the interaction potential is the foundation of molecular dynamics simulations, governing the movement, interactions, and properties of particles within a simulated system. Choosing an appropriate interaction potential is crucial for accurately representing the thermodynamic properties as well as the structural evolution of materials. Some of these

empirical potentials can be named, such as, two- and three-body interactions in functional form [19–22], two- and three-body interactions in separate form [23–27]. In this study, the interactions between boron (B) and nitrogen (N) in armchair BNNR are described by Tersoff potential [28]. This potential energy includes contributions from various interactions, such as bonded interactions (e.g., covalent bonds) and non-bonded interactions (e.g., van der Waals forces, electrostatic interactions). The Tersoff potential is written as below:

$$E_b = \frac{1}{2} \sum_{i \neq j} f_c(r_{ij}) [f_R(r_{ij}) + b_{ij} f_a(r_{ij})] \quad (1)$$

In which, r_{ij} represent the distance from atom i to atom j . B_{ij} is a many-body coupling between the bond from atom i to atom j and the local environment of atom i . The repulsive $f_R(r_{ij})$ and the attractive $f_a(r_{ij})$ terms are considered based on Morse potential as proposed by Brenner [26]. The $f_c(r_{ij})$ term is a cutoff function using for calculating the number of neighbors as well as making the potential to zero outside the interaction shell.

The software package Large-Scale Atomic/Molecular Massively Parallel Simulator is used to perform the MD simulation [29]. The ring distribution following the ‘shortest path’ rule is calculated using ISAACS software [30]. For 2D visualization of atomic configurations, VMD software is applied [31]. The temperature of system is added following a linear rule: $T = T_0 + \gamma t$, in which $T_0 = 50$ K and γ is a heating rate, t is a time required for heating. All configurations are relaxed for 6×10^5 MD steps before analyzing the structural characteristics or 2D visualization to make sure the stability of the models. It is important to note that each MD step corresponds to a time interval of 0.0001 picoseconds.

Firstly, the initial configurations are relaxed in the isothermal-isobaric ensemble for 6×10^5 MD steps at $T_0 = 50$ K under periodic boundary conditions. Then, non-periodic boundary conditions with an elastic reflection behavior are applied along the armchair edge after adding the empty space of 20 Å at both ends. At this stage, initial configurations are relaxed again to reach equilibrium for 6×10^5 MD steps at $T_0 = 50$ K using canonical ensemble simulation. Finally, the initial configurations are heated up to about 6000 K, which is higher than the melting point of zigzag h-BNNR [18] to make sure that the armchair h-BNNR is completely in a liquid state at that value of temperature. Note that the heating rate is K/s .

3. Results and discussion

As is well-known, the total energy-per-atom landscape determines the stable configurations of the system. At equilibrium, particles are positioned to minimize the total energy per atom. However, the total energy-per-atom minima may shift as the system’s temperature changes. By analyzing the total energy per atom, one can identify stable conformations, energy barriers, and phase changes such as solid-to-liquid, providing insights into the stability and dynamics of molecular processes. In this study, the total energy per atom for each configuration (10000, 20000, and 30000 atoms) is calculated and presented in Fig. 1.

Overall, the behavior of the total energy of each atom of three configurations exhibits the same behavior (Fig. 1). That is: i) At low temperatures, the total energy of each atom initially increases linearly. The reason is that in the low-temperature region, the vibrations of the atoms are only around the equilibrium position; ii) Next, when the temperature increases to a large enough

value (this temperature value depends on the size of the configuration which is calculated by the heat capacity as below), the total energy of each atom suddenly jumps. This sudden increase of energy is because the vibration amplitude of the atoms is too large, leading to the breakage of the bonds between atoms. This proves that there is a phase transition from the crystalline state to the liquid state of the model; iii) Finally, the total energy per atom is linear again in the high-temperature region. At this temperature range, the bonds between atoms are broken leading to the formation of the liquid state of the model. As well-known, a first-order phase transition refers to a phase transition in which there is a direct conversion between two distinct phases of matter, such as solid to liquid, liquid to gas, or vice versa. This type of phase transition is characterized by abrupt changes in certain thermodynamic properties, discontinuities in the order parameters, and the release or absorption of latent heat. Therefore, in this study, the phase transition from a crystal to a liquid state for 10000-atom, 20000-atom, and 30000-atom configurations exhibits a first-order.

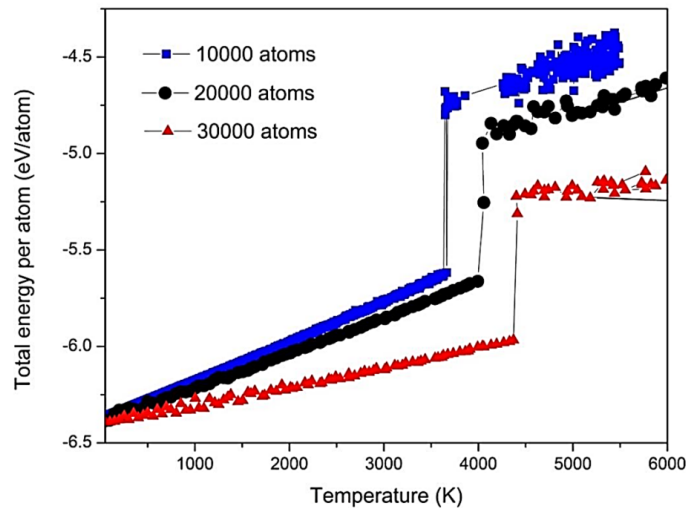


Fig. 1. Temperature dependence of total energy per atom in case of 4.3×10^{12} K/s: 10000-atom armchair h-BNNR – square symbol, 20000-atom armchair h-BNNR – circle symbol, and 30000-atom armchair h-BNNR – triangle symbol.

As for the 10000-atom armchair h-BNNR (square symbol in Fig. 1), the sudden increase in the total energy of each atom occurs at a temperature below 4000 K. Related to the 20000-atom configuration (circle symbol in Fig. 1), the direct conversion between two distinct phases of h-BNNR is around 4000 K. As regards the 30000-atom armchair h-BNNR (triangle symbol in Fig. 1), the phase transition from crystal to liquid happens at a temperature above 4000 K. One can conclude that the temperature of the phase transition from a crystal to a liquid state of armchair h-BNNR depends on the initial configuration size. This temperature shifts to the higher zone in the increase in the size of the initial configuration due to some reasons such as the edge effects. As well known that the edge atoms have fewer neighboring atoms, leading to altered mechanical properties near the edges. As the size of the initial configuration decreases, edge effects become more prominent, affecting its overall behavior including the melting point. In addition, at smaller

sizes, the initial configuration's response to strain may differ from that of larger samples due to size-dependent deformation mechanisms. Note that the melting temperature of zigzag h-BNNR containing 10000 atoms is 4522 K which is higher than that of armchair h-BNNR [18]. This may be due to the dangling bonds at the edges of the h-BNNR armchair.

As seen, the graph of the total energy per atom will give us an overview of the phase transition process from crystal to liquid state at the temperature range without specifying the melting temperature point. Therefore, to determine the value of the melting temperature point, the heat capacity quantity is investigated. As is well known, heat capacity is a crucial parameter in understanding the thermal behavior and energetics of molecular systems in MD simulations, and it provides valuable information about how a system responds to temperature changes and undergoes phase transitions. To determine the specific phase transition temperature point of each h-BNNR configuration, the heat capacity is calculated according to the expression:

$$C = \frac{\Delta E}{\Delta T}. \quad (2)$$

As regards the 10000-atom h-BNNR configuration (Fig. 2a), the peak of the heat capacity stays at a temperature of 3640 K showing that the melting point is 3640 K. As for the 20000-atom h-BNNR configuration (Fig. 2b), the phase transition from a crystal to a liquid state is at 4000 K based on the peak of the heat capacity. Related to the 30000-atom h-BNNR configuration (Fig. 2c), the graph of the heat capacity reaches the maximum height at 4400 K indicating that the melting point is 4400 K. Thus, it can be seen that the melting temperature of armchair h-BNNR depends on the size of the initial configuration in the range of this study. Melting temperature tends to increase with increasing configuration size.

The rate dependence of the melting process in MD simulations offers insights into how the speed of heating influences the kinetics, pathways, and structural changes associated with the transition from solid to liquid phases. The heating rate refers to how quickly the temperature of the system is increased during the simulation. Slower heating rates may allow the material to equilibrate more effectively during the heating process, leading to more organized melting and better-defined nucleation of the liquid phase. However, there will be a problem with the timescales of MD simulations, which are limited by computational resources. Faster heating rates might lead to more disordered melting and reduced nucleation times. In addition, higher heating rates can lead to superheating, where the temperature of the solid phase exceeds its equilibrium melting point before melting occurs. This is because the system doesn't have enough time to transition to the liquid phase. Superheating can be useful in scientific research to understand phase transition kinetics, nucleation processes, and metastable states of materials.

In this study, we consider the superheating case with two heating rates for the 20000-atom armchair h-BNNR configuration: the pentagon symbol in Fig. 3 is 1.5×10^{12} K/s, circle symbol in Fig. 3 is 4.3×10^{12} K/s, the triangle symbol in Fig. 3 is 7.5×10^{12} K/s, and the square symbol in Fig. 3 is 10^{13} K/s. One can see that the phase transition of the armchair h-BNNR with all heating rates exhibits a first-order. However, the melting point of the armchair h-BNNR from a crystal to a liquid state depends on the heating rates. Details about the melting points of the 20000-atom case are calculated through the heat capacity: the melting point at the heating rate of K/s is about 4000 K as shown in Fig. 2b) while the one at 1.5×10^{12} K/s is about 3600 K as shown in Fig. 4. Continuing to increase the heating rate to 7.5×10^{12} K/s (triangle symbol in Fig. 4) and

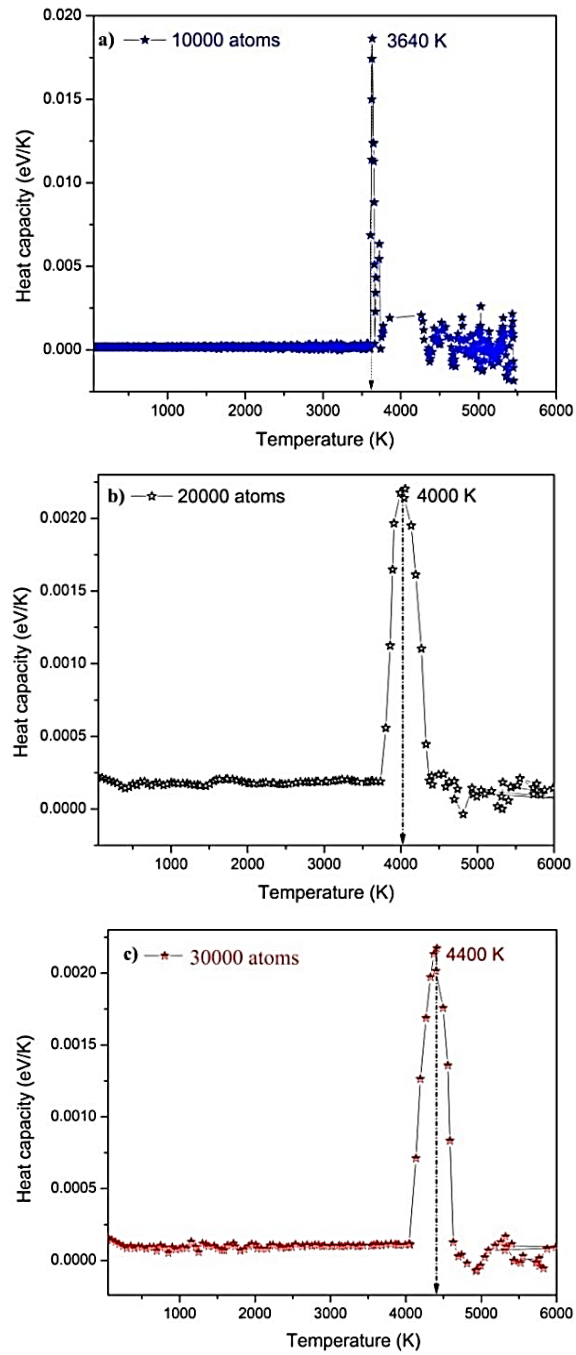


Fig. 2. The temperature dependence of the heat capacity in case of 4.3×10^{12} K/s: a) 10000-atom h-BNNR configuration; b) 20000-atom h-BNNR configuration; c) 30000-atom h-BNNR configuration.

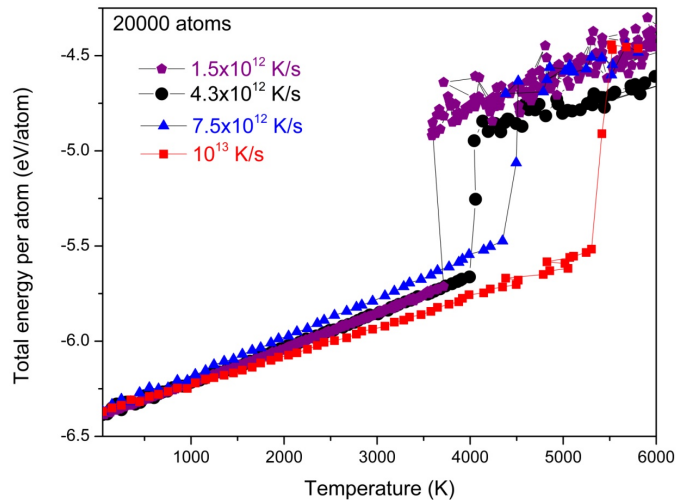


Fig. 3. Temperature dependence of total energy per atom of 20000-atom armchair h-BNNR configuration: 1.5×10^{12} K/s – pentagon symbol, 4.3×10^{12} K/s – circle symbol, 7.5×10^{12} K/s – triangle symbol, 10^{13} K/s – square symbol.

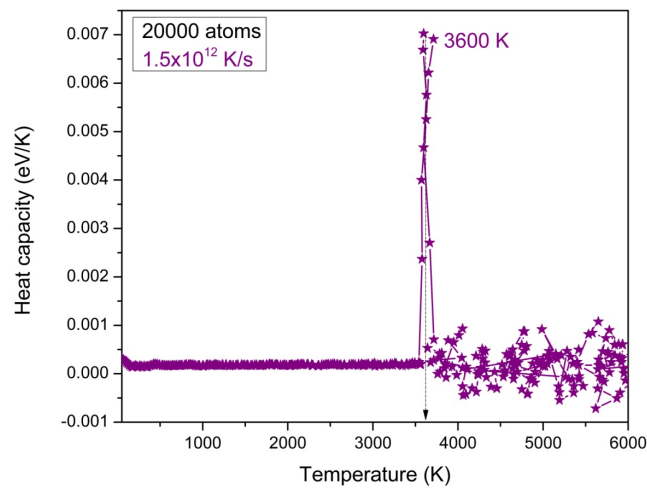


Fig. 4. The temperature dependence of the heat capacity for the 20000-atom h-BNNR configuration at 1.5×10^{12} K/s.

10^{13} K/s (square symbol in Fig. 4), the melting temperature increases to about 4500 K and 5400 K, respectively (Fig. 4). This shows that, in this study range, the melting point of the 20000-atom armchair h-BNNR configuration increases as the heating rate increases. This has many causes, and

one of them may be a consequence of superheating. As mentioned above, when a crystal is heated rapidly, there may not be enough time for the material to equilibrate, leading to non-equilibrium conditions. As a result, the observed melting point differs from the melting equilibrium point under slower heating rates.

To study the atomic mechanism of melting process, the parameter is calculated and used to observe the appearance of liquid-like atoms upon heating. The parameter is written as below:

$$\Psi_6 = \frac{1}{N} \sum_{a=1}^N \Psi_{6,p}^a \quad (3)$$

where, N is total atom in the configuration, $\Psi_{6,p}^a$ is described as below:

$$\Psi_{6,p}^a = \frac{1}{p} \sum_{b=1}^p e^{i6\theta_{a,b}} \quad (4)$$

In which, a is the chosen atom, p is the number of the nearest atoms to the chosen atom a , and $\theta_{a,b}$ is the angle between the chosen atom a and the nearest atoms.

Ψ_6 is often used to assess the hexatic order in a system and quantifies the local orientation of particles concerning their neighbors. A higher value of Ψ_6 indicates a stronger alignment of neighboring particles, implying a higher degree of order or crystalline-like structure. In contrast, a lower value of Ψ_6 suggests that the arrangement of particles is more disordered and lacks the regularity associated with crystalline structures. Thus, the state of the material at a lower value of Ψ_6 can be considered a liquid state.

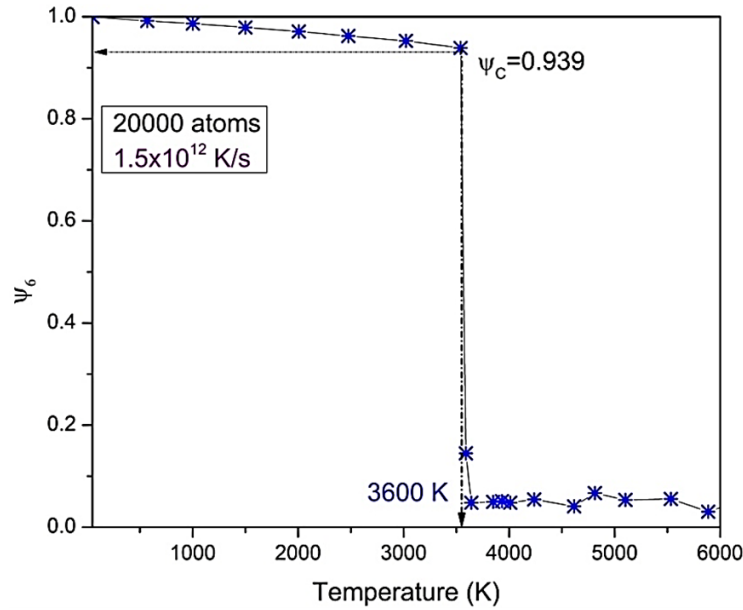


Fig. 5. The temperature dependence of the parameter for the 20000-atom h-BNNR configuration at 1.5×10^{12} K/s.

In this study, the Ψ_6 parameter is calculated and presented in Fig. 5. One can see that at temperatures below 3600 K, the value of Ψ_6 is nearly 1 indicating a crystalline-like structure of the armchair h-BNNR configuration. After that the value Ψ_6 of decreases significantly to nearly zero at temperatures higher than 3600 K. This indicates that there is a phase transition from a crystal to a liquid state at 3600 K. This result is similar to the one of total energy of each atom in Fig. 4. In this sense, the value of Ψ_6 just before dropping to zero can be considered critical value denoted as Ψ_C . In this study, Ψ_C is about 0.939.

To classify solid atoms and liquid atoms, Ψ_6 can be used as follows: atoms with $\Psi_6 > 0.5$ are considered liquid-like atoms and conversely, atoms with $\Psi_6 < 0.5$ are considered solid-like atoms. The appearance of liquid-like atoms is calculated and presented in Fig. 6.

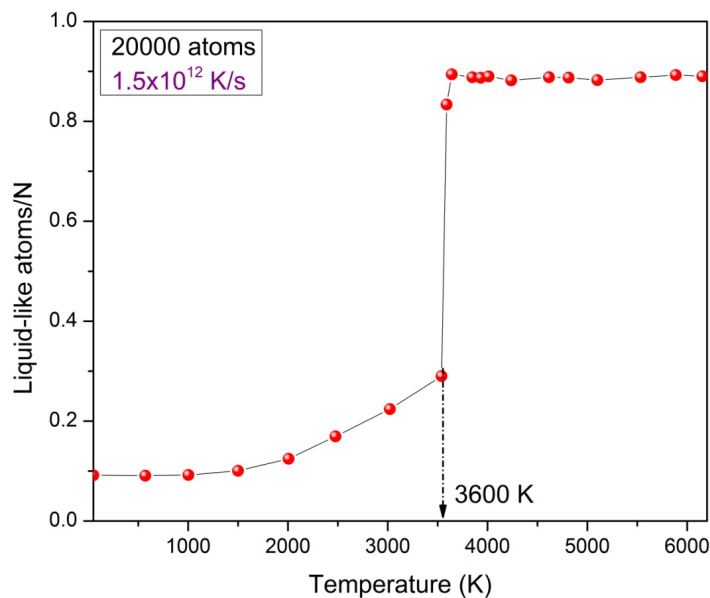


Fig. 6. The temperature dependence of the appearance of liquid-like atoms for the 20000-atom h-BNNR configuration at 1.5×10^{12} K/s (N is total atoms in the configurations).

At temperatures from 50 K to 1500 K, there are a small number of liquid-like atoms that are located at the edges because the atoms at the edges are unpaired or unsatisfied chemical bonds. Upon heating to just before 3600 K, the number of liquid-like atoms increases slightly and linearly from 0.1 to 0.287 as shown in Fig. 6. These liquid atoms first appear at the edges and then start growing inward. At 3600 K, the number of liquid-like atoms increases sharply from 0.287 to 0.83 and to 0.9 at 3640 K and higher. Thus, at the phase transition temperature, almost the entire crystal structure of the armchair h-BNNR configuration collapses. This can be visually observed in Fig. 7. At a temperature of 3500 K, the interior of the configuration still has crystalline structures (Fig. 7a). However, at the phase transition temperature of 3600 K, these crystal structures break down (Fig. 7b).

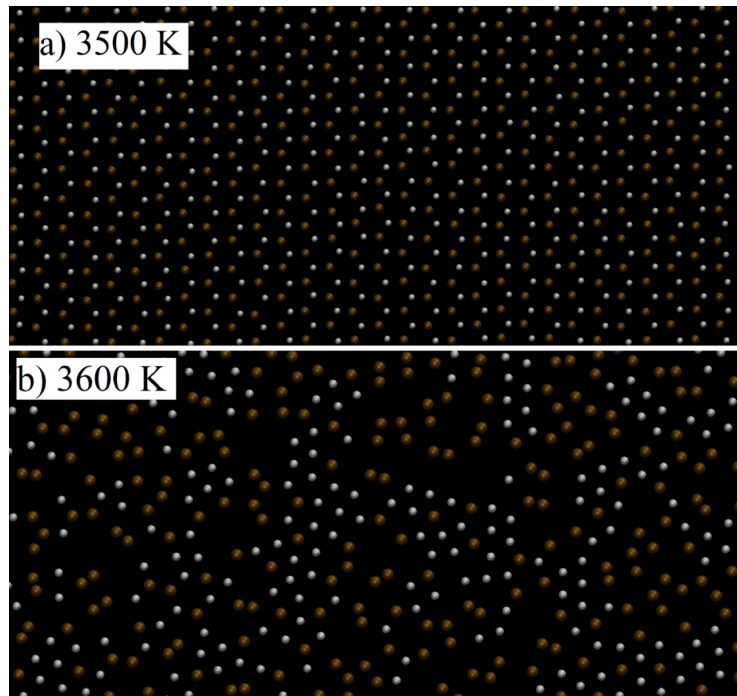


Fig. 7. Two-dimensional view of 20000-atom h-BNNR configuration at 1.5×10^{12} K/s: a) 3500 K, b) 3600 K.

4. Conclusion

The dependence of the armchair h-BNNR configuration on the size and the heating rate is studied using a comprehensive MD simulation. The Tersoff potential is applied for the interactions between B and N in the configuration. Some results are named as follows:

- Three configuration sizes (10.000, 20.000, and 30.000 atoms) of the armchair h-BNNR are considered. The phase transition of all sizes of the armchair h-BNNR from a crystal to a liquid state exhibits a first-order type. In this study range, the melting points are defined based on the calculation of the heat capacity increase as the initial configuration size increases. The melting points of 10.000, 20.000, and 30.000 atoms are 3640 K, 4000 K, and 4400 K, respectively.
- The dependence on the heating rate of the armchair h-BNNR is considered for the case of 20000 atoms. The melting points of two heating rates of K/s, K/s, K/s, and K/s are 3600 K, 4000 K, 4500 K, and 5400 K, respectively. In this study range, the melting point decreases as the heating rate decreases.
- The atomic mechanism of the melting process is studied by analyzing the parameter and the appearance of the liquid-like atoms based on the critical value. The critical value is used to classify solid-like and liquid-like atoms. The appearance of liquid-like atoms upon heating starts from the edges and grows inward. At the phase transition

temperature, almost the entire crystal structure of the armchair h-BNNR configuration collapses.

References

- [1] L. Liu, Y. Feng, and Z. Shen, *Structural and electronic properties of h-BN*, Phys. Rev. B, **68** (2003) 104102.
- [2] A. Bozkurt, G.Ö. Çakal, Ş. Kaya-Keleş, and A. Kaşkaş, *Comparison of h-BN material with metal implants in radiotherapy applications: Characterization and dose distribution measurements in LINAC*, Radiat. Phys. Chem. **212** (2023) 111152.
- [3] S. Ngamprapawat, J. Kawase, T. Nishimura, K. Watanabe, T. Taniguchi, and K. Nagashio, *From h-BN to Graphene: Characterizations of Hybrid Carbon-Doped h-BN for Applications in Electronic and Optoelectronic Devices*, Adv. Electron. Mater. **9** (2023) 2300083.
- [4] H. Liu, J. Qin, X. Yang, C. Lv, W. Huang, F. Li, C. Zhang, Y. Wu, L. Dong, and C. Shan, *Highly sensitive humidity sensors based on hexagonal boron nitride nanosheets for contactless sensing*, Nano Res. **16** (2023) 10279.
- [5] A. Kiakojoury, I. Frank, and E. Nadimi, *Exploring the dynamics of DNA nucleotides in graphene/h-BN nanopores: insights from ab initio molecular dynamics*, Phys. Chem. Chem. Phys. **25** (2023) 13452.
- [6] H. Li, W. Sheng, S.A. Haruna, Q. Bei, W. Wei, M.M. Hassan, and Q. Chen, *Recent progress in photoelectrochemical sensors to quantify pesticides in foods: Theory, photoactive substrate selection, recognition elements and applications*, TRAC-Trend. in Anal. Chem. **164** (2023) 117108.
- [7] M. Chae, D. Lee, S. Kim, and H.-d. Kim, *NO Sensing Properties of BN-based Memristor Sensor Array for Real-time NO Monitoring-Systems*, Sens. Actuators B Chem. **394** (2023) 134373.
- [8] M. Qiu, Z. Jia, M. Yang, K. Nishimura, C.-T. Lin, N. Jiang, and Q. Yuan, *High detectivity solar blind photodetector based on mechanical exfoliated hexagonal boron nitride films*, Nanotechnology, **34** (2023) 285204.
- [9] S. Kim, B. Kim, S. Park, W.S. Chang, H. Kang, S. Kim, H. Lee, and S. Kim, *Hysteretic behavior of all CVD h-BN/graphene/h-BN heterostructure field-effect transistors by interfacial charge trap*, Surf. Interfaces **36** (2023) 102615.
- [10] S. Abdous, M. Derradji, Z. Mekhalif, K. Khiari, O. Mehelli, and Y.B. Cherif, *Advances in Polymeric Neutron Shielding: The Role of Benzoxazine-h-BN Nanocomposites in Nuclear Protection*, Radiat. Res. **394** (2023) 134373.
- [11] P.A. Drózdź, M. Haras, A. Przewłoka, A. Krajewska, M. Filipiak, M. Słowikowski, B. Stonio, K. Czerniak-Łosiewicz, Z. Mierczyk, and T. Skotnicki, *A graphene/h-BN MEMS varactor for sub-THz and THz applications*, Nanoscale, **15** (2023) 12530.
- [12] Z. Wang, L. Wei, S. Wang, T. Wu, L. Sun, C. Ma, X. Tao, and S. Wang, *2D SiP₂/h-BN for a Gate-Controlled Phototransistor with Ultrahigh Sensitivity*, ACS Appl. Mater. Interfaces **15** (2023) 15810.
- [13] R. Wang, J. Lu, X. Wu, J. Peng, and J.-H. Jiang, *Topological Transitions Enhance the Performance of Twisted Thermophotovoltaic Systems*, Phys. Rev. Appl. **19** (2023) 044050.
- [14] H.T. Nguyen, *Structural evolution of in-plane hybrid graphene/hexagonal boron nitride heterostructure upon heating*, J. Mol. Graph. Model. **125** (2023) 108579.
- [15] Q. Fang, Z. Pang, Q. Ai, Y. Liu, T. Zhai, D. Steinbach, G. Gao, Y. Zhu, T. Li, and J. Lou, *Superior mechanical properties of multilayer covalent-organic frameworks enabled by rationally tuning molecular interlayer interactions*, Proc. Natl. Acad. Sci. **120** (2023) e2208676120.
- [16] L. Gong, H. Shi, S. He, J. Yang, Q. Han, Y. Ren, Y. Zhao, and Z. Jiang, *Thermal conductivity and interfacial thermal conductivity of complex boron nitride nanoribbons*, J. Therm. Stresses **46** (2023) 198.
- [17] R. Yogi and N.K. Jaiswal, *Adsorption of CO gas molecules on zigzag BN/AlN nanoribbons for nano sensor applications*, Phys. Lett. A **383** (2019) 532.
- [18] H.T. Nguyen and T.T.T. Hanh, *Melting process of zigzag boron nitride nanoribbon*, Physica E Low Dimens. Syst. Nanostruct. **106** (2019) 95.
- [19] M.Z. Bazant, E. Kaxiras, and J.F. Justo, *Environment-dependent interatomic potential for bulk silicon*, Phys. Rev. B, **56** (1997) 8542.
- [20] J.F. Justo, M.Z. Bazant, E. Kaxiras, V.V. Bulatov, and S. Yip, *Interatomic potential for silicon defects and disordered phases*, Phys. Rev. B **58** (1998) 2539.

- [21] N. Marks, *Generalizing the environment-dependent interaction potential for carbon*, Phys. Rev. B **63** (2000) 035401.
- [22] F.H. Stillinger and T.A. Weber, *Computer simulation of local order in condensed phases of silicon*, Phys. Rev. B **31** (1985) 5262.
- [23] J. Tersoff, *New empirical model for the structural properties of silicon*, Phys. Rev. Lett. **56** (1986) 632.
- [24] B.W. Dodson, *Development of a many-body Tersoff-type potential for silicon*, Phys. Rev. B **35** (1987) 2795.
- [25] J. Tersoff, *New empirical approach for the structure and energy of covalent systems*, Phys. Rev. B **37** (1988) 6991.
- [26] D.W. Brenner, *Tersoff-type potentials for carbon, hydrogen and oxygen*, MRS Online Proceedings Library (OPL) **141** (1988).
- [27] J.R. Chelikowsky and J. Phillips, *Surface and thermodynamic interatomic force fields for silicon clusters and bulk phases*, Phys. Rev. B **41** (1990) 5735.
- [28] J. Tersoff, *Modeling solid-state chemistry: Interatomic potentials for multicomponent systems*, Phys. Rev. B **39** (1989) 5566.
- [29] S. Plimpton, *Fast parallel algorithms for short-range molecular dynamics*, J. Comput. Phys. **117** (1995) 1.
- [30] S. Le Roux and V. Petkov, *ISAACS—interactive structure analysis of amorphous and crystalline systems*, J. Appl. Crystallogr. **43** (2010) 181.
- [31] W. Humphrey, A. Dalke, and K. Schulten, *VMD: visual molecular dynamics*, J. Mol. Graphics, **14** (1996) 33.